



OPEN

Effect of the molar ratio of (Ni²⁺ and Fe³⁺) on the magnetic, optical and antibacterial properties of ternary metal oxide CdO–NiO–Fe₂O₃ nanocomposites

Asma A. A. Al-Mushki¹, Abdullah A. A. Ahmed^{1✉}, A. M. Abdulwahab¹, Salem A. S. Qaid^{1,2}, Nasser S. Alzayed², Mohammed Shahabuddin², Jameel M. A. Abduljalil³ & Fuad A. A. Saad³

In this work, the effect of the molar ratio of (Ni²⁺ and Fe³⁺) on the properties of CdO–NiO–Fe₂O₃ nanocomposites was investigated. The synthesis of CdO–NiO–Fe₂O₃ nanocomposites was carried out by self-combustion. XRD, UV–Vis, PL and VSM were used to describe the physical properties of the materials. The results showed significant progress in structural and optical properties supporting antibacterial activity. For all samples, the particle size decreased from 28.96 to 24.95 nm with increasing Ni²⁺ content and decreasing Fe³⁺ content, as shown by the XRD pattern, which also shows the crystal structure of cubic CdO, cubic NiO, and cubic γ-Fe₂O₃ spinel. The Ni²⁺ and Fe³⁺ contents in the CdO–NiO–Fe₂O₃ nanocomposites have also been shown to enhance the ferromagnetic properties. Due to the significant coupling between Fe₂O₃ and NiO, the coercivity H_c values of the samples increase from 66.4 to 266 Oe. The potential of the nanocomposites for antibacterial activity was investigated against Gram-positive (*Staphylococcus aureus*) and Gram-negative (*Pseudomonas aeruginosa*, *Escherichia coli*, and *Moraxella catarrhalis*) bacteria. Comparison of *P. aeruginosa* with *E. coli*, *S. aureus* and *M. catarrhalis* showed that it has a stronger antibacterial activity with a ZOI of 25 mm.

The synthesis of nanomaterials is at the heart of the current research field of nanotechnology, which offers a wide range of interesting applications, e.g. in the fields of electrochemistry, biomedicine, catalysis, cosmetics, electronics, optics and optical devices, energy science, mechanics, food technology, healthcare, sensors, textile technology, space technology and pharmaceuticals^{1–8}.

CdO is a well-known n-type semiconductor with piezoelectric properties and polycrystalline nature^{4,9}. As a result, cadmium oxide nanoparticles (CdO NPs) are extensively used in various applications, including photovoltaic cells, photodiodes, transparent electrodes, gas sensors, infrared detectors, liquid crystal displays, antireflective coatings, and solar cells^{10–13}. CdO is an excellent photocatalyst for photocatalytic applications due to its ability to absorb visible light and its high carrier mobility^{14,15}. Due to their unusual physiochemical properties, CdO NPs are effective against malaria, bacteria, tuberculosis, and cancer^{4,9,16}.

Fe₂O₃, an environmentally friendly semiconducting oxide material, is widely used in biomedicine, catalysts, and batteries. Apart from these applications, Fe₂O₃ is a promising candidate for a variety of technological applications¹⁷. Fe₂O₃ has shown promise for applications such as drug delivery, organic impurity removal, and MRI imaging^{18,19}. Due to its high surface-to-volume ratio, Fe₂O₃ with nanometric dimensions exhibits modified properties^{20,21}. Due to their superparamagnetic properties, nontoxicity, and biocompatibility, they are becoming increasingly popular. It is promising as catalytic material, absorbent, magnetic recording device, ion exchanger, gas sensor and other applications. Iron oxide is the most stable and environmentally friendly oxide in the world^{22–24}.

¹Department of Physics, Faculty of Applied Science, Thamar University, 87246 Dhamar, Yemen. ²Department of Physics and Astronomy, College of Science, King Saud University, PO Box 2455, Riyadh 11451, Saudi Arabia. ³Department of Biology, Faculty of Applied Science, Thamar University, 87246 Dhamar, Yemen. ✉email: abdullah2803@gmail.com

NiO is one of the most important transition metal oxides with a wide range of properties when reacting with polar surface materials and is used in a variety of applications due to its excellent chemical and thermal stability, antibacterial activity, environmental friendliness and industrial use²⁵.

The capabilities of the individual metal oxides have been greatly enhanced by combining them into innovative nanocomposites, opening up new possibilities for applications in photocatalysis, electro- and optoelectronics, and biology²⁶.

The synthesis of CdO–NiO–ZnO nanocomposites for photocatalytic and antibacterial properties was discussed by Karthik et al. Together with tested foodborne pathogens, the nanocomposite showed strong antibacterial activity²⁷. Karthik et al. have reported CdO–NiO nanocomposites. The composite showed significant antibacterial activity against foodborne pathogens²⁸. Tushar et al. reported the antibacterial activity of α -Fe₂O₃-ZnO in the core shell²⁹. Balamurugan et al. reported the preparation of CdO–Al₂O₃-NiO nanocomposites for photocatalytic and magnetic properties. The composite exhibited weak ferrimagnetic assemblies, making it suitable for magnetic applications³⁰. Gnanamoorthy et al. have reported rGO/ZnCo₂O₄ nanocomposites and x-CuTiAP nanospheres for antimicrobial applications. The nanocomposites showed antimicrobial activity^{31,32}.

This work aims to investigate the effects of the conditions for the preparation of CdO–NiO–Fe₂O₃ nanocomposites by the self-combustion method on the structural, optical, magnetic and antibacterial activity.

Experiment

Materials. Cadmium nitrate tetrahydrate (Cd(NO₃)₂·4H₂O, Scharlau, 99%), nickel nitrate hexahydrate (Ni(NO₃)₂·6H₂O, Fluka, 98%), iron nitrate nonahydrate (III) (Fe(NO₃)₃·9H₂O, Scharlau, extra pure), polyvinyl alcohol cold water soluble ((-CH₂CHOH-)_n, HIMEDIA, 99.99%), and deionized water (DW) were used for the present work. The chemical materials were used in this work without further purification.

Sample preparation. The CdO–NiO–Fe₂O₃ nanocomposites were prepared by the self-combustion method³³. Briefly, dissolve 5 g of PVA in 200 ml of DW, followed by vigorous stirring for 2 h at 50 °C. The PVA solution was obtained as a gel-like and homogeneous solution. This solution was donated by solution A. Different ratios of nickel and iron, while cadmium was kept constant (Table 1), was prepared separately in 3 solutions. At room temperature, the solution was stirred for 10 min to obtain a homogeneous transparent solution. The solutions of Ni nitrate, Fe nitrate and Cd nitrate were mixed with constant stirring for another 10 min at room temperature. The product solutions were mixed with solution A for 20 min with constant stirring. The stirred solutions were placed in the drying oven for 3 h at 80 °C. The crushed products were calcined at 500 °C for 2 h.

Characterizations. X-ray diffraction (XRD) was used to investigate the structural features of the fabricated samples (XD-2 X-ray diffractometer with Cu K α (λ = 1.54 at 36 kV and 20 mA, China). A UV–Vis spectrophotometer (SPECORD 200) was used to measure the absorption spectra of the samples in the range of 190–1100 nm at room temperature. A spectrofluorometer (RF-5301PC; Shimadzu) with an excitation wavelength of 325 nm, an excitation and emission gap of 5 nm, an average scanning speed, and high sensitivity was used to record the photoluminescence spectra (PL) of the fabricated samples. The physical property measurement system (PPMS), QUANTUM DESIGN (MODEL6000), was used together with the attached vibrating magnetometer (VSM) to obtain the magnetic hysteresis (M–H) loops. The solvent for the prepared samples used to measure the absorption and photoluminescence spectra was dilute sulfuric acid (H₂SO₄).

Antibacterial activity. The modified Kirby-Bauer disk diffusion test of the European Committee for Antimicrobial Susceptibility Testing was used to investigate the antibacterial activities of CdO–NiO–Fe₂O₃ nanocomposites against Gram-positive (*Staphylococcus aureus*) and Gram-negative (*Pseudomonas aeruginosa*, *Escherichia coli*, and *Moraxella catarrhalis*) bacteria³⁴. Biochemical assays were used to further verify the identity of the isolates before testing the nanocomposites. The nanocomposites were serially diluted twice from the 75 mg/ml stock solution and suspended in sterile distilled water. The disks were impregnated with four different working dilutions. 450, 225, 112.5, and 56.25 μ g/disk were prepared by impregnating a sterile filter paper disk (6 mm diameter) with 12 μ l (6 μ l on each side) for dilution. The plates were inoculated with swabs to form a uniform bacterial lawn on the agar surface. Using sterile forceps, the plates were positioned on the infected agar surface and incubated for 18–20 h at 37 °C. After completion of the incubation period, the diameters of the inhibition zones were measured to the nearest millimeter. In addition to the disks containing azithromycin as a positive control, a blank disk consisting solely of distilled water was used as a negative control.

Sample code	Molar ratio of salts (M)			Weight of salts (g) at 100 ml of DW			Molar ratio of PVA (g/ml)
	Cd ²⁺	Ni ²⁺	Fe ³⁺	Cd ²⁺	Ni ²⁺	Fe ³⁺	
CNF1	0.2	0.05	0.15	4.6	1.1	4.6	0.025
CNF2	0.2	0.1	0.1	4.6	2.2	3.03	0.025
CNF3	0.2	0.15	0.05	4.6	3.3	1.52	0.025

Table 1. Samples code at various molar ratio of Ni²⁺ and Fe³⁺.

Result and discussion

XRD analysis. The crystal structure of the CdO–NiO–Fe₂O₃ nanocomposite was investigated using the XRD technique. In Fig. 1, the XRD patterns of the prepared nanocomposites show only the crystalline phase of CdO, NiO and Fe₂O₃ for all samples. The patterns show the face-centered cubic structure of CdO and NiO, while Fe₂O₃ exhibits pure maghemite (γ -Fe₂O₃ phase with a cubic spinel crystal structure). The CdO patterns at 2 θ and its crystal plane at 33°(111), 38.3°(200), 55.34°(220), 65.94°(311), and 69.34°(311) correspond to JCPDS Map No. 00-005-0640³⁵. The NiO patterns at 2 θ and its crystal plane at 37.18°(111), 43.30°(200), and 63.04°(220) are consistent with JCPDS Map No. 47-1049³⁶. The patterns of the γ -Fe₂O₃ phases at 2 θ and their crystal plane at 30.2°(206), 35.5°(119), and 57.2°(115) are consistent with JCPDS Map No. 00-025-1402³⁷. It is clear that the intensity of the peaks of γ -Fe₂O₃ decreases with decreasing Fe content, while the intensity of the peaks of NiO increases with increasing Ni content.

The XRD data obtained indicate that an increase in Ni²⁺ and a decrease in Fe³⁺ content causes a change in crystal lattice parameters and a decrease in crystallite size, as indicated in Table 2.

The Scherrer equation^{38–43} is used to calculate the average crystal size of nanocomposites in the crystal plane of CdO (111), which can be given as follows:

$$D = \frac{K\lambda}{\beta \cos\theta} \quad (1)$$

where K is the dimensionless form factor (K = 0.9), λ is the X-ray wavelength (= 0.1540 nm), β is the full width at half maximum (FWHM), and θ is the Bragg diffraction angle.

The microstrain (ϵ) of a nanocrystal is caused by defects in the nanocrystal, such as distortions and imperfections. The microstrain can be calculated using the following equation (ϵ)^{43–45}:

$$\epsilon = \frac{\beta}{4 \tan\theta} \quad (2)$$

the dislocation density can be described by the following equation (δ)^{39,43,45,46}:

$$\delta = \frac{1}{D^2} \quad (3)$$

As seen in Table 2, the particle size decreased from 28.96 to 24.95 nm with increasing Ni²⁺ and decreasing Fe³⁺ content. The decrease in particle size of nanocomposites is attributed to the difference between the ionic radii of

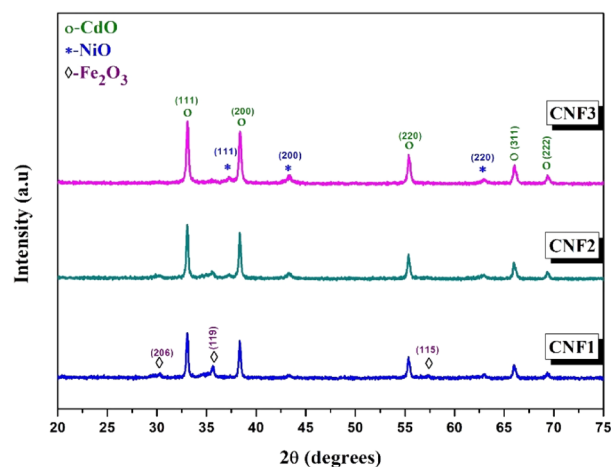


Figure 1. XRD patterns of CdO–NiO–Fe₂O₃ nanocomposites at various molar ratio of Ni²⁺ and Fe³⁺. The figure exhibited the crystallization of the oxides an increase as the molar ratio different from CNF1 to CNF3.

Samples	Unit cell parameter, <i>a</i> (nm)			D (nm)	$\epsilon \times 10^{-3}$	$\delta \times 10^{-3}$ (nm ⁻²)
	CdO [fcc]	NiO [fcc]	Fe ₂ O ₃ [fcc]			
CNF1	0.4697	0.4173	0.834	28.95	4.22	1.19
CNF2	0.4690	0.4176	0.835	26.89	4.54	1.38
CNF3	0.4690	0.4175	0.834	24.94	4.90	1.61

Table 2. The Unit cell parameter (*a*), average crystalline size (D), lattice strain (ϵ) and the dislocation density (δ) of CdO–NiO–Fe₂O₃ nanocomposites at various molar ratio of Ni²⁺ and Fe³⁺.

Ni (0.074 nm), Cd (0.097 nm) and Fe (0.055 nm)⁴⁷. The dependence of particle size on dislocation density and microstrain. The values of microstrain and dislocation density increase due to the large effect of particle size on the comprehensive stress of the nanocomposite⁴⁸.

Optical properties. *Absorption spectra.* The absorption spectra of CdO–NiO–Fe₂O₃ nanocomposites at different molar ratios of Ni²⁺ and Fe³⁺ were studied in the wavelength range of (200–800 nm) as shown in Fig. 2. The absorption peaks observed at 213–260 nm are attributed to the absorption band of CdO, while the absorption peaks observed at 310–320 nm are attributed to the absorption band of NiO in the nanocomposite⁴⁶. In special CNF1 samples, a tiny absorption band at 530 nm was observed for Fe₂O₃. This absorption band is caused by the absorption of Fe²⁺ and Fe³⁺ ions of iron oxide⁴⁹.

Band gap energy (E_g). As seen from Table 3 and Fig. 3, the optical band gap (E_g) of the samples is between NiO (3.6 eV)⁵⁰, CdO (2.5 eV)^{51,52} and Fe₂O₃ (2 eV)⁵³. For the samples, the optical band gap (E_g) increased with increasing Ni²⁺ content and with decreasing Fe³⁺ content. The decrease in band gap is related to the grain size. As localized energy states emerge and approach the conduction band, the energy band gap decreases in nanocomposites with a high content of Cd²⁺^{46,48}.

PL study. Figure 4 shows the PL spectra of CdO–NiO–Fe₂O₃ nanocomposites at 325 nm and room temperature. The near band edge (NBE) emission of NiO nanoparticles in a nanocomposite matrix was responsible for the observed UV emission peak at 359 nm⁵⁴. Radiative recombination is responsible for the NBE peak in NiO in the exciton-exciton collision process⁵⁵. The trapped electrons migrating into the valence band at the Ni interstitial are thought to be responsible for the strong violet emission peaks at 408 and 423 nm⁴⁰. In CdO–NiO–Fe₂O₃ nanocomposites, band gap defects such as oxygen vacancies were responsible for the weak blue emission peaks between 463 and 494 nm^{56,57}.

Magnetic properties. VSM was used to analyze the magnetic properties of CdO–NiO–Fe₂O₃ nanocomposites at room temperature. Using a magnetic field of 10,000 Oe, magnetic hysteresis measurements were performed on CdO–NiO–Fe₂O₃ nanocomposites. As shown in Fig. 5, all samples exhibit ferromagnetic properties, which can be attributed to the presence of Fe₂O₃ in all three samples. The CdO–NiO–Fe₂O₃ nanocomposites showed weak ferromagnetism as the measured particle size was above the critical value (10 nm)^{58,59}. The values of saturation magnetization (M_s) decrease from 0.482 to 0.060 emu with increasing Ni²⁺ content and decreasing Fe³⁺ content in the samples due to the antiferromagnetic property of NiO and ferromagnetic nature of Fe₂O₃^{60,61}. The coercivity H_c of the samples increases from 66.4 to 266 Oe, which can be attributed to the strong coupling

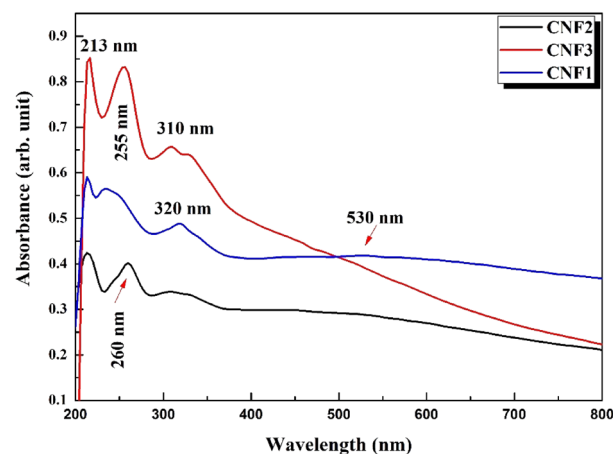


Figure 2. Absorbance spectra of CdO–NiO–Fe₂O₃ nanocomposites at various molar ratio of Ni²⁺ and Fe³⁺. The figure showed the absorption peaks for oxides.

Samples	Energy band gap, E _g (eV)
CNF1	2.71
CNF2	2.74
CNF3	2.87

Table 3. Optical band gap energy measurements of CdO–NiO–Fe₂O₃ nanocomposites at various molar ratio of Ni²⁺ and Fe³⁺.

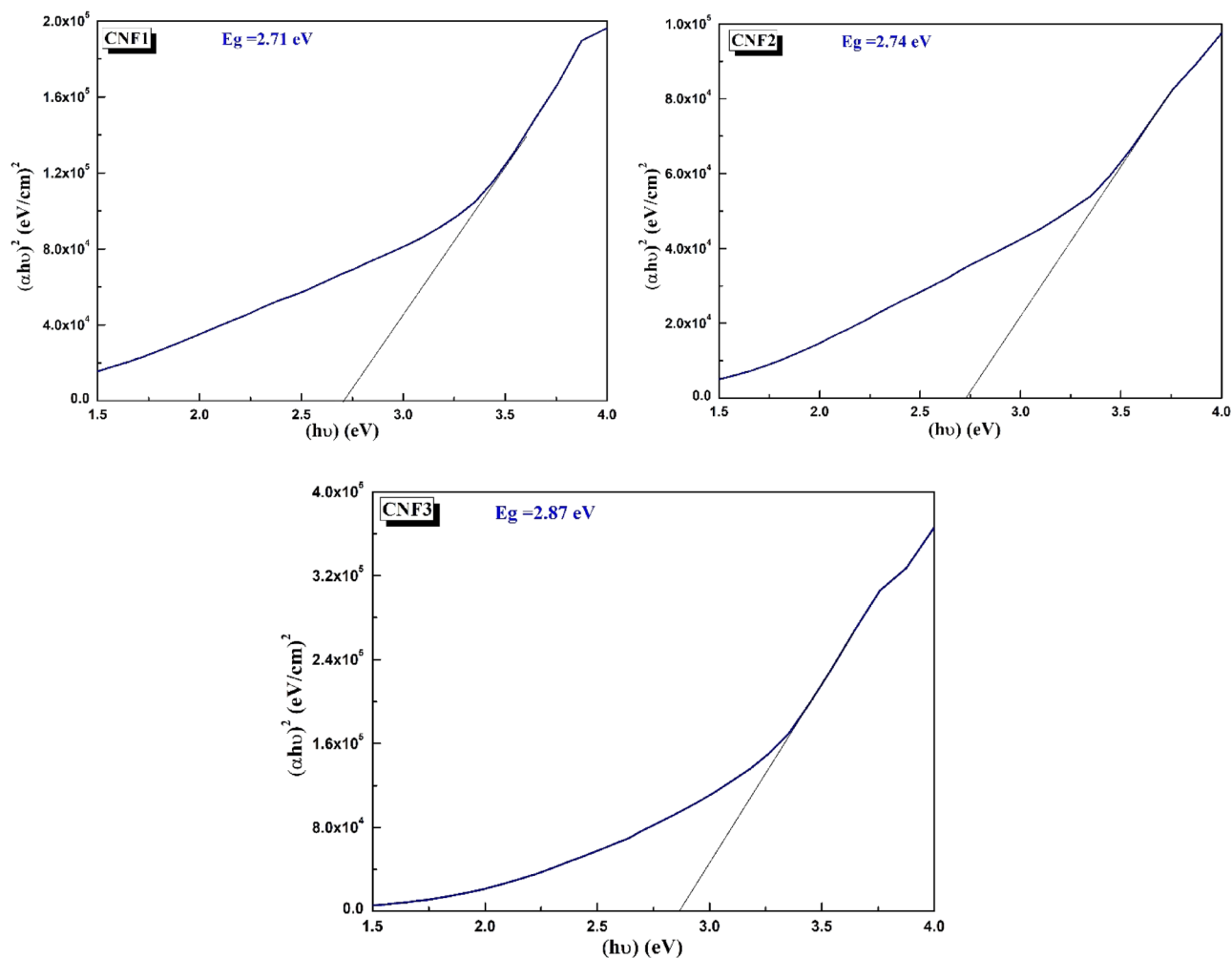


Figure 3. Optical band gap of CdO–NiO–Fe₂O₃ nanocomposites at various molar ratio of Ni²⁺ and Fe³⁺.

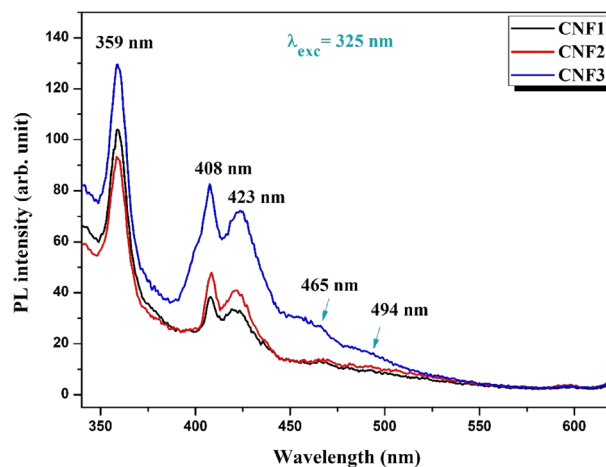


Figure 4. PL spectrum of CdO–NiO–Fe₂O₃ nanocomposites at various molar ratio of Ni²⁺ and Fe³⁺.

between Fe₂O₃ and NiO⁶². It has been shown that the content of Ni²⁺ and Fe³⁺ in the CdO–NiO–Fe₂O₃ nanocomposites increases the ferromagnetic properties. The ferromagnetism of the CdO–NiO–Fe₂O₃ nanocomposites was increased at room temperature by replacing the nonmagnetic Cd with the magnetic transition metal ions Ni²⁺ and Fe³⁺. Moreover, the ferromagnetism of the nanocomposites increased when oxygen vacancies were formed in them^{15,63}. Thus, the causes of the ferromagnetic properties of the metal oxides are the presence of

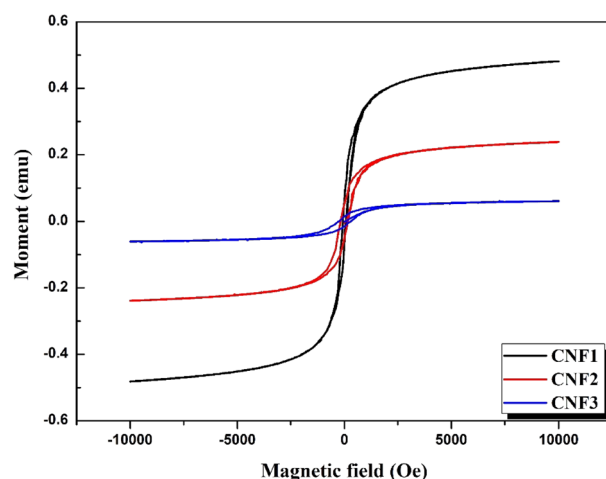


Figure 5. Magnetic hysteresis curves of CdO–NiO–Fe₂O₃ nanocomposites at various molar ratio of Ni²⁺ and Fe³⁺. The figure showed variation of the coercivity (H_c), and saturation magnetization (M_s) as the molar ratio different from CNF1 to CNF3.

unpaired electron spins arising from surface effects, oxygen/cation vacancies on the surfaces of the samples, and/or the presence of a secondary/impure phase^{15,58}. The magnetic parameters (H_c , M_r , and M_s) are listed in Table 4.

Antibacterial activity. The antibacterial properties of the CdO–NiO–Fe₂O₃ nanocomposites were investigated against Gram-positive bacteria (*S. aureus*) and Gram-negative bacteria (*M. catarrhalis*, *E. coli*, and *P. aeruginosa*) (see Figs. 6, 7). The CdO–NiO–Fe₂O₃ nanocomposites are present at concentrations ranging from 56.25 to 450 µg/ml. The zone of inhibition (ZOI), which illustrates how the CdO–NiO–Fe₂O₃ nanocomposites affect bacterial growth, is shown in Figs. 6 and 7. The dramatic effects at 450 µg/ml were clearly visible. The ZOI of the CdO–NiO–Fe₂O₃ nanocomposites against the bacterial strains *E. coli*, *P. aeruginosa*, *S. aureus* and *M. catarrhalis* is 14, 25, 20 and 22 nm, respectively. In reality, the metal nanoparticles bind to the proteins and DNA of the pathogens by interacting with vital components such as the phosphorus (P) and sulphur (S) groups of bacterial DNA. As a result, bacterial DNA replication is destroyed⁶⁴. One possible mechanism for the antibacterial effect is the production of free radicals. Through the damaged surface, the Cd²⁺, Ni²⁺ and Fe³⁺ ions in the nanocomposites penetrate the cell walls of the pathogens. Reactive oxygen species (ROS) are formed when ions are released from the nanoparticles. Superoxide radicals, hydroxyl radicals, singlet oxygen, and hydrogen peroxide are just some of the ROS components that have significant bactericidal activity^{65–71}. The ZOI in this study compared with other studies is shown in Table 5.

Conclusion

In conclusion, the preparation of CdO–NiO–Fe₂O₃ was successful, and its physical and antibacterial properties were studied. The molar ratio of Ni²⁺ and Fe³⁺ can affect the average crystallite size (D_{av}), dislocation density (δ) and microstrain (ϵ). In particular, the results showed that the coupling of CdO with NiO and Fe₂O₃ improved the magnetic properties of CdO. At room temperature, the ferromagnetism of the CdO–NiO–Fe₂O₃ nanocomposites was enhanced, making them suitable for magnetic applications. According to the results, the grown nanocomposite showed high performance as antibacterial activity for various Gram-negative and positive bacteria, which could be a strong candidate for bacterial disinfection.

Sample	Coercivity (Oe)	Remanent (emu)	Saturation magnetization (emu)
CNF1	66.4	0.0632	0.482
CNF2	176	0.0511	0.238
CNF3	266	0.0140	0.060

Table 4. Magnetic coercivity (H_c), remanent magnetization (M_r), and saturation magnetization (M_s) of CdO–NiO–Fe₂O₃ nanocomposites at various molar ratio of Ni²⁺ and Fe³⁺.

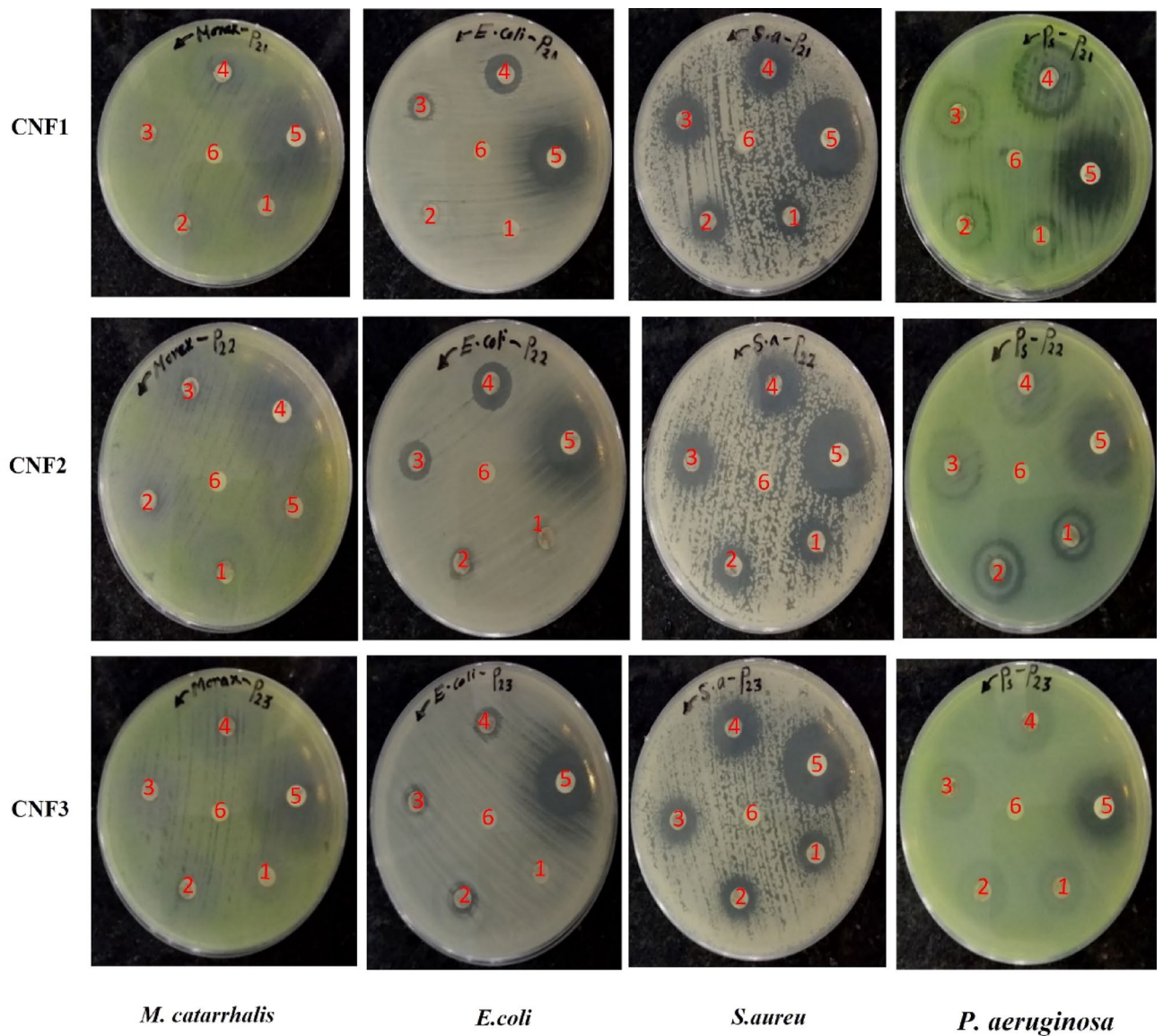


Figure 6. Antibacterial activity of CdO–NiO–Fe₂O₃ nanocomposites against bacteria: (*M. catarrhalis*), (*E. coli*), (*S. aureus*) and (*P. aeruginosa*). (1) 56.25, (2) 112.5, (3) 225 and (4) 450 µg/ml per disk of nanocomposites, (5) Azithromycin antibiotics (positive control) and (6) distilled water (negative control).

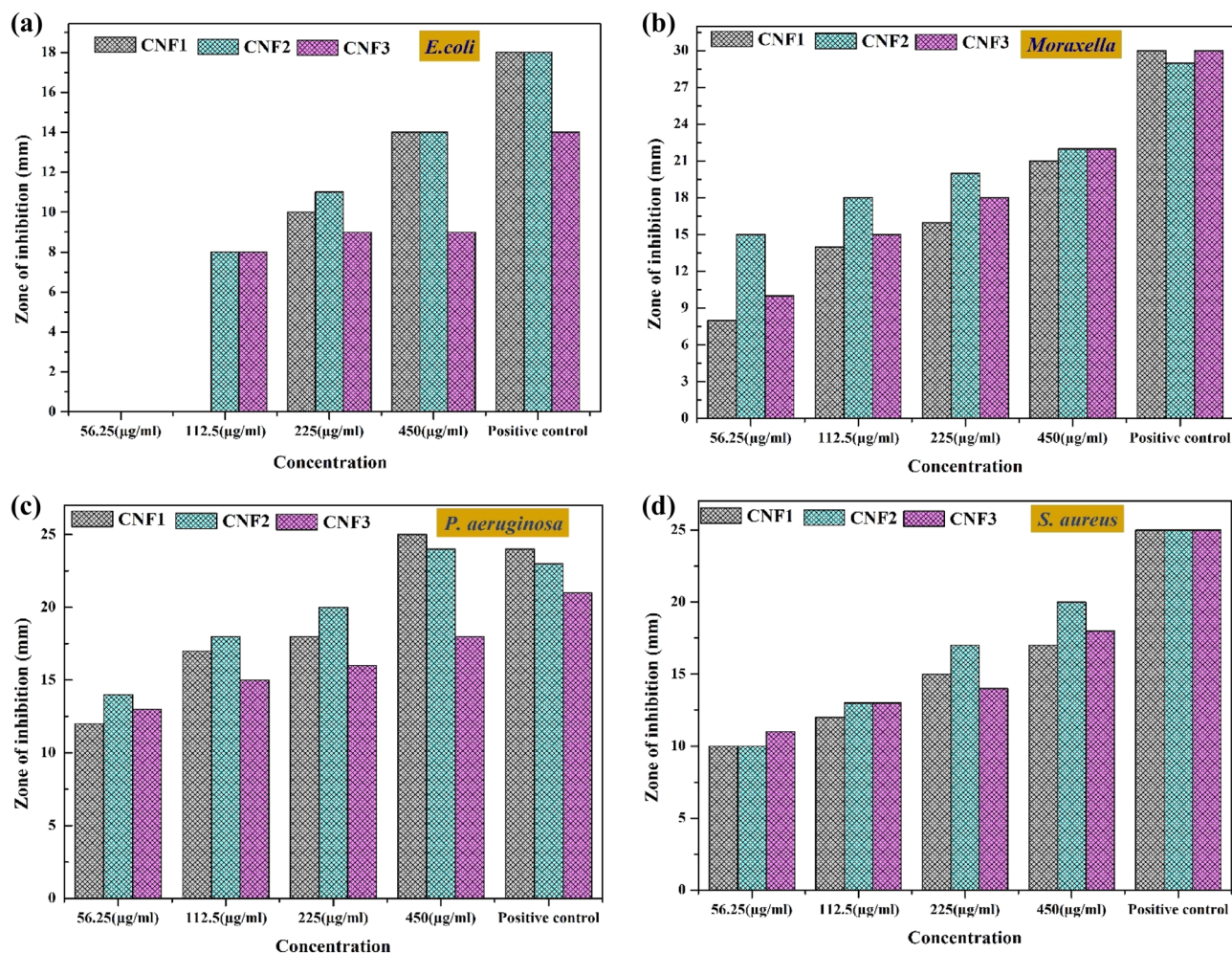


Figure 7. ZOI against (a) *E. coli*, (b) *Moraxella*, (c) *P. aeruginosa*, and (d) *S. aureus* bacterial strains in the presence of CNF1, CNF2 and CNF3 nanocomposites. The figure showed specialty of prepared nanocomposites, the CNF2 has a significant impact on bacteria compared to CNF1 and CNF3.

Nanoparticles (NPs)	Assessment method	Target bacteria				References
		<i>Escherichia coli</i>	<i>Staphylococcus aureus</i>	<i>Pseudomonas aeruginosa</i>	<i>Moraxella catarrhalis</i>	
CuO–MgO–ZnO	ZOI (mm), 1 mg/µL	26	19	22	–	72
CeO ₂ –CuO–ZnO	ZOI (mm), 50 µg/µL	10	14	12	–	73
CdO–ZnO–MgO	ZOI (mm), 100 µg/mL	23	–	22	–	35
CdO–NiO–Fe ₂ O ₃	ZOI (mm), 450 µg/ml	13	25	25	25	67
CdO–NiO–Fe ₂ O ₃	ZOI (mm), 450 µg/ml	18	23	25	25	68
Ag–CuO	ZOI (mm), 20 µg/mL	2.1	0.75	–	–	74
AgI–CdO	ZOI (mm), 50 mg/ml	20	20	29	–	75
CS–MgO	MIC	11.9 µg/mL	9.8 µg/mL	–	–	76
CS–NiO	MIC	3.86 µg/mL	2.11 µg/mL	–	–	76
MgO	ZOI (mm), 20 µg/mL	6.8	7.2	–	–	65
NiO	ZOI (mm), 1 mg/mL	17.2	16.5	18.2	–	77
Polyoxotungstate (POT)	MIC	–	–	–	1 µg/mL	78
Aristolochia bracteolate	ZOI (mm)	–	–	–	12	79
CdO–NiO–Fe ₂ O ₃	ZOI (mm), 450 µg/ml	14	25	20	22	Present work

Table 5. A comparison of antibacterial activity of CdO–NiO–Fe₂O₃ nanocomposites with some other metal oxide nanocomposites, metal oxides and compounds.

Data availability

The authors confirm that the data supporting the findings of this study are available within the article.

Received: 4 April 2023; Accepted: 31 May 2023

Published online: 03 June 2023

References

- Bera, A. & Belhaj, H. Application of nanotechnology by means of nanoparticles and nanodispersions in oil recovery—A comprehensive review. *J. Nat. Gas. Sci. Eng.* **34**, 1284–1309 (2016).
- Frewer, L. J. *et al.* Consumer attitudes towards nanotechnologies applied to food production. *Trends Food Sci. Technol.* **40**, 211–225 (2014).
- Ghosh Chaudhuri, R. & Paria, S. Core/shell nanoparticles: Classes, properties, synthesis mechanisms, characterization, and applications. *Chem. Rev.* **112**, 2373–2433 (2012).
- Ghotekar, S. A review on plant extract mediated biogenic synthesis of CdO nanoparticles and their recent applications. *Asian J. Green Chem.* **3**, 187–200 (2019).
- Ghotekar, S. K. *et al.* Biosynthesis of silver nanoparticles using unripe fruit extract of *Annona reticulata* L. and its characterization. *World J. Pharm. Pharm. Sci.* **4**, 1304–1312 (2015).
- Hussein, A. K. Applications of nanotechnology to improve the performance of solar collectors—Recent advances and overview. *Renew. Sustain. Energy Rev.* **62**, 767–792 (2016).
- Syedmoradi, L. *et al.* Point of care testing: The impact of nanotechnology. *Biosens. Bioelectron.* **87**, 373–387 (2017).
- Vélez, M. A., Perotti, M. C., Santiago, L., Gennaro, A. M. & Hynes, E. in *Nutrient delivery* 221–250 (Elsevier, 2017).
- Heidari, A. & Brown, C. Study of composition and morphology of cadmium oxide (CdO) nanoparticles for eliminating cancer cells. *J. Nanomed. Res.* **2**, 20 (2015).
- Campos-González, E. *et al.* Structural and optical properties of CdTe-nanocrystals thin films grown by chemical synthesis. *Mater. Sci. Semicond. Process.* **35**, 144–148 (2015).
- Mansoor, M. *et al.* Cadmium-manganese oxide composite thin films: Synthesis, characterization and photoelectrochemical properties. *Mater. Chem. Phys.* **186**, 286–294 (2017).
- Rajesh, N., Kannan, J., Leonardi, S., Neri, G. & Krishnakumar, T. Investigation of CdO nanostructures synthesized by microwave assisted irradiation technique for NO₂ gas detection. *J. Alloys Compd.* **607**, 54–60 (2014).
- Thema, F., Beukes, P., Gurib-Fakim, A. & Maaza, M. Green synthesis of Montepoint CdO nanoparticles by *Agathosma betulina* natural extract. *J. Alloys Compd.* **646**, 1043–1048 (2015).
- Tadjarodi, A., Imani, M. & Kerdari, H. Experimental design to optimize the synthesis of CdO cauliflower-like nanostructure and high performance in photodegradation of toxic azo dyes. *Mater. Res. Bull.* **48**, 935–942 (2013).
- Nallendran, R., Selvan, G. & Balu, A. NiO coupled CdO nanoparticles with enhanced magnetic and antifungal properties. *Surf. Interfaces* **15**, 11–18 (2019).
- Salehi, B., Mortaz, E. & Tabarsi, P. Comparison of antibacterial activities of cadmium oxide nanoparticles against *Pseudomonas Aeruginosa* and *Staphylococcus Aureus* bacteria. *Adv. Biomed. Res.* **4**, 105 (2015).
- Abaker, M. *et al.* A highly sensitive ammonia chemical sensor based on α -Fe₂O₃ nanoellipsoids. *J. Phys. D* **44**, 425401 (2011).
- Gangopadhyay, P., Gallet, S., Franz, E., Persoons, A. & Verbiest, T. Novel superparamagnetic core (shell) nanoparticles for magnetic targeted drug delivery and hyperthermia treatment. *IEEE Trans. Magn.* **41**, 4194–4196 (2005).
- Yan, S. *et al.* Therapeutic effect of Fe₂O₃ nanoparticles combined with magnetic fluid hyperthermia on cultured liver cancer cells and xenograft liver cancers. *J. Nanosci. Nanotechnol.* **5**, 1185–1192 (2005).
- Sharma, S., Dhiman, N., Kumar, A., Singh, M. & Dhiman, P. Effect of synthesis method on optical and magnetic properties of Fe₂O₃ nanoparticles. *Integr. Ferroelectr.* **204**, 38–46 (2020).
- Zahn, M. Magnetic fluid and nanoparticle applications to nanotechnology. *J. Nanopart. Res.* **3**, 73–78 (2001).
- Cao, D., He, P. & Hu, N. Electrochemical biosensors utilising electron transfer in heme proteins immobilised on Fe₃O₄ nanoparticles. *Analyst* **128**, 1268–1274 (2003).
- Feldmann, C. Preparation of nanoscale pigment particles. *Adv. Mater.* **13**, 1301–1303 (2001).
- Wen, X., Wang, S., Ding, Y., Wang, Z. L. & Yang, S. Controlled growth of large-area, uniform, vertically aligned arrays of α -Fe₂O₃ nanobelts and nanowires. *J. Phys. Chem. B* **109**, 215–220 (2005).
- Ali, H., Tiama, T. M. & Ismail, A. New and efficient NiO/chitosan/polyvinyl alcohol nanocomposites as antibacterial and dye adsorptive films. *Int. J. Biol. Macromol.* **186**, 278–288 (2021).
- Rodríguez, J. *et al.* Studies on the behavior of mixed-metal oxides and desulfurization: reaction of H₂S and SO₂ with Cr₂O₃ (0001), MgO (100), and Cr₂Mg_{1-x}O (100). *J. Am. Chem. Soc.* **122**, 12362–12370 (2000).
- Kannan, K. *et al.* Photocatalytic and antimicrobial properties of microwave synthesized mixed metal oxide nanocomposite. *Inorg. Chem. Commun.* **125**, 108429 (2021).
- Karthik, K. & Dhanuskodi, S. in *AIP conference proceedings*. 050021 (AIP Publishing LLC).
- Jana, T. K. *et al.* The antibacterial and anticancer properties of zinc oxide coated iron oxide nanotextured composites. *Colloids Surf. B* **177**, 512–519 (2019).
- Balamurugan, S. *et al.* Multi metal oxide CdO–Al₂O₃–NiO nanocomposite—Synthesis, photocatalytic and magnetic properties. *Mater. Res. Express* **6**, 015022 (2018).
- Gnanamoorthy, G. *et al.* Realization of rGO/ZnCo₂O₄ nanocomposites enhanced for the antimicrobial, electrochemical and photocatalytic activities. *Diam. Relat. Mater.* **120**, 108677 (2021).
- Gnanamoorthy, G. *et al.* New orchestrated of X-CuTiAP (en, trien, ETA and DMA) nanospheres with enhanced photocatalytic and antimicrobial activities. *J. Ind. Eng. Chem.* **110**, 503–519 (2022).
- Seibert, O., Grégr, J. & Kejzlar, P. The preparation of iron oxide nanoparticles by a self-combustion method. *Manuf. Technol.* **19**, 680–684 (2019).
- Kahlmeter, G., Brown, D., Goldstein, F., MacGowan, A., Mouton, J., Odenholt, I., Rodloff, A., Soussy, C. J., Steinbakk, M. & Soriano, F. Vol. 12 501–503 (Wiley Online Library, 2006).
- Revathi, V. & Karthik, K. Microwave assisted CdO–ZnO–MgO nanocomposite and its photocatalytic and antibacterial studies. *J. Mater. Sci. Mater. Electron.* **29**, 18519–18530 (2018).
- Jana, S., Mondal, A. & Ghosh, A. Fabrication of stable NiO/Fe₂O₃ heterostructure: A versatile hybrid material for electrochemical sensing of glucose, methanol and enhanced photodecomposition and/photoreduction of water contaminants. *Appl. Catal. B* **232**, 26–36 (2018).
- Iqbal, J. *et al.* Biogenic synthesis of green and cost effective iron nanoparticles and evaluation of their potential biomedical properties. *J. Mol. Struct.* **1199**, 126979 (2020).
- Karthik, K., Dhanuskodi, S., Gobinath, C. & Sivaramakrishnan, S. Microwave-assisted synthesis of CdO–ZnO nanocomposite and its antibacterial activity against human pathogens. *Spectrochim. Acta A Mol. Biomol. Spectrosc.* **139**, 7–12 (2015).

39. El-Fadl, A. A. *et al.* Syntheses of new spinels $Zn_{1-x}Fe_xAl_2O_4$ nanocrystallines structure: Optical and magnetic characteristics. *J. Alloys Compd.* **795**, 114–119 (2019).
40. Munawar, T., Iqbal, F., Yasmeen, S., Mahmood, K. & Hussain, A. Multi metal oxide NiO–CdO–ZnO nanocomposite–synthesis, structural, optical, electrical properties and enhanced sunlight driven photocatalytic activity. *Ceram. Int.* **46**, 2421–2437 (2020).
41. Scherrer, P. Bestimmung der inneren Struktur und der Grobe von Kolloidteilchen mittels Röntgenstrahlen. *Göttinger Nachr. Ges.* **2** (1918).
42. Vorokh, A. S. Scherrer formula: Estimation of error in determining small nanoparticle size. *Наносистемы: физика, химия, математика* **9**, 364–369 (2018).
43. Afify, N. Syntheses of new (CdO)(1-X)(NiO) XZnO nanocomposite system: Preparation, structure, and magnetic properties. *Mater. Sci. Eng. B* **273**, 115399 (2021).
44. Balzar, D. *et al.* Size–strain line-broadening analysis of the ceria round-robin sample. *J. Appl. Crystallogr.* **37**, 911–924 (2004).
45. Thamri, S., Sta, I., Jlassi, M., Hajji, M. & Ezzaouia, H. Fabrication of ZnO–NiO nanocomposite thin films and experimental study of the effect of the NiO, ZnO concentration on its physical properties. *Mater. Sci. Semicond. Process.* **71**, 310–320 (2017).
46. Karthik, K., Dhanuskodi, S., Gobinath, C., Prabukumar, S. & Sivaramakrishnan, S. Multifunctional properties of microwave assisted CdO–NiO–ZnO mixed metal oxide nanocomposite: enhanced photocatalytic and antibacterial activities. *J. Mater. Sci. Mater. Electron.* **29**, 5459–5471 (2018).
47. Thambidurai, S., Gowthaman, P., Venkatachalam, M. & Suresh, S. Enhanced bactericidal performance of nickel oxide-zinc oxide nanocomposites synthesized by facile chemical co-precipitation method. *J. Alloys Compd.* **830**, 154642 (2020).
48. Zeid, E. F. A., Ibrahim, I. A., Ali, A. M. & Mohamed, W. A. The effect of CdO content on the crystal structure, surface morphology, optical properties and photocatalytic efficiency of p-NiO/n-CdO nanocomposite. *Results Phys.* **12**, 562–570 (2019).
49. Rahman, A. *et al.* Structural, optical and photocatalytic studies of trimetallic oxides nanostructures prepared via wet chemical approach. *Synth. Met.* **259**, 116228 (2020).
50. Aftab, M., Butt, M., Ali, D., Bashir, F. & Khan, T. M. Optical and electrical properties of NiO and Cu-doped NiO thin films synthesized by spray pyrolysis. *Opt. Mater.* **119**, 111369 (2021).
51. Mosquera, E., del Pozo, I. & Morel, M. Structure and red shift of optical band gap in CdO–ZnO nanocomposite synthesized by the sol gel method. *J. Solid State Chem.* **206**, 265–271 (2013).
52. Katubi, K. M. *et al.* Synthesis and characterization of graphitic carbon nitride composite with $NiFe_2O_4/CdO$ for photocatalytic treatment of diclofenac sodium and crystal violet. *Opt. Mater.* **139**, 113721 (2023).
53. Seo, O. *et al.* Tuning of structural, optical band gap, and electrical properties of room-temperature-grown epitaxial thin films through the Fe_2O_3 : NiO ratio. *Sci. Rep.* **9**, 4304 (2019).
54. Gandhi, A. C. & Wu, S. Y. Strong deep-level-emission photoluminescence in NiO nanoparticles. *Nanomaterials* **7**, 231 (2017).
55. Subhan, M. A., Ahmed, T., Uddin, N., Azad, A. K. & Begum, K. Synthesis, characterization, PL properties, photocatalytic and antibacterial activities of nano multi-metal oxide NiO– CeO_2 –ZnO. *Spectrochim. Acta A Mol. Biomol. Spectrosc.* **136**, 824–831 (2015).
56. Nallendran, R., Selvan, G. & Balu, A. Photoconductive and photocatalytic properties of CdO–NiO nanocomposite synthesized by a cost effective chemical method. *J. Mater. Sci. Mater. Electron.* **29**, 11384–11393 (2018).
57. Nallendran, R., Selvan, G. & Balu, A. CdO– Fe_2O_4 nanocomposite with enhanced magnetic and photocatalytic properties. *Mater. Sci. Poland* **37**, 100–107 (2019).
58. Arun, L., Karthikeyan, C., Philip, D. & Unni, C. Optical, magnetic, electrical, and chemo-catalytic properties of bio-synthesized CuO/NiO nanocomposites. *J. Phys. Chem. Solids* **136**, 109155 (2020).
59. Narsinga Rao, G., Yao, Y. & Chen, J. Evolution of size, morphology, and magnetic properties of CuO nanoparticles by thermal annealing. *J. Appl. Phys.* **105**, 093901 (2009).
60. Bhushan, M., Kumar, Y., Periyasamy, L. & Viswanath, A. K. Fabrication and a detailed study of antibacterial properties of $\alpha-Fe_2O_3$ /NiO nanocomposites along with their structural, optical, thermal, magnetic and cytotoxic features. *J. Nanotechnol.* **30**, 185101 (2019).
61. He, X.-M., Zhang, C.-W., Guo, F.-F., Yan, S.-M., Li, Y.-T., Liu, L.-Q., Zhang, H.-G., Du, Y.-W. & Zhong, W. J. P. C. P. Exchange-biased hybrid $\gamma-Fe_2O_3$ /NiO core-shell nanostructures: Three-step synthesis, microstructure, and magnetic properties. *Phys. Chem. Chem. Phys.* **21**, 11967–11976 (2019).
62. Skoropata, E., Su, T., Ouyang, H., Freeland, J. & van Lierop, J. J. P. R. B. Intermixing enables strong exchange coupling in nanocomposites: Magnetism through the interfacial ferrite in $\gamma-Fe_2O_3$ /NiO. *Phys. Rev. B* **96**, 024447 (2017).
63. Meneses, C., Duque, J., Vivas, L. & Knobel, M. Synthesis and characterization of TM-doped CuO (TM = Fe, Ni). *J. Non Cryst. Solids* **354**, 4830–4832 (2008).
64. Mani, M. *et al.* Systematic green synthesis of silver oxide nanoparticles for antimicrobial activity. *Environ. Res.* **202**, 111627 (2021).
65. Ahmad, A., Khan, M., Khan, S., Luque, R., Almutairi, T. & Karami, A. Bio-construction of MgO nanoparticles using Texas sage plant extract for catalytic degradation of methylene blue via photocatalysis. *Int. J. Environ. Sci. Technol.* 1–12 (2022).
66. Wagner, C., Zatzko, D. & Raymond, R. Use of the oxygen KLL Auger lines in identification of surface chemical states by electron spectroscopy for chemical analysis. *Adv. Anal. Chem* **52**, 1445–1451 (1980).
67. Ahmed, A. A. *et al.* Effect of ethylene glycol concentration on the structural and optical properties of multimetal oxide CdO–NiO– Fe_2O_3 nanocomposites for antibacterial activity. *J. Phys. Chem. Solids* **155**, 110113 (2021).
68. Al-Mushki, A. A. *et al.* Structural, optical, and antibacterial characteristics of mixed metal oxide CdO–NiO– Fe_2O_3 nanocomposites prepared using a self-combustion method at different polyvinyl alcohol concentrations. *Appl. Phys. A* **128**, 1–15 (2022).
69. Kannan, K., Radhika, D., Nesaraj, A., Sadasivuni, K. K. & Krishna, L. S. Facile synthesis of NiO–CYSO nanocomposite for photocatalytic and antibacterial applications. *Inorg. Chem. Commun.* **122**, 108307 (2020).
70. Kannan, K., Radhika, D., Gnanasangeetha, D., Krishna, L. S. & Gurushankar, K. Y3+ and Sm3+ co-doped mixed metal oxide nanocomposite: Structural, electrochemical, photocatalytic, and antibacterial properties. *Appl. Surf. Sci.* **4**, 100085 (2021).
71. Kannan, K. *et al.* Facile fabrication of novel ceria-based nanocomposite (CYO–CSO) via co-precipitation: Electrochemical, photocatalytic and antibacterial performances. *J. Mol. Struct.* **1256**, 132519 (2022).
72. Munawar, T. *et al.* Sunlight-induced photocatalytic degradation of various dyes and bacterial inactivation using CuO–MgO–ZnO nanocomposite. *Environ. Sci. Pollut. Res.* **28**, 42243–42260 (2021).
73. Subhan, M. A., Uddin, N., Sarker, P., Azad, A. K. & Begum, K. Photoluminescence, photocatalytic and antibacterial activities of CeO_2 –CuO–ZnO nanocomposite fabricated by co-precipitation method. *Spectrochim. Acta A Mol. Biomol. Spectrosc.* **149**, 839–850 (2015).
74. Parvathiraja, C. & Shailajha, S. Bioproduction of CuO and Ag/CuO heterogeneous photocatalysis-photocatalytic dye degradation and biological activities. *Appl. Nanosci.* **11**, 1411–1425 (2021).
75. Warshagha, M. Z., Muneer, M., Althagafi, I. I. & Ahmed, S. A. Highly efficient and stable AgI–CdO nanocomposites for photocatalytic and antibacterial activity. *RSC Adv.* **13**, 5013–5026 (2023).
76. Mizwari, Z. M., Oladipo, A. A. & Yilmaz, E. Chitosan/metal oxide nanocomposites: Synthesis, characterization, and antibacterial activity. *Int. J. Polym. Mater. Polym. Biomater* **70**, 383–391 (2021).
77. Alam, M. W. *et al.* Effect of Mo doping in NiO nanoparticles for structural modification and its efficiency for antioxidant, antibacterial applications. *Sci. Rep.* **13**, 1328 (2023).
78. Gumerova, N. I. *et al.* Antibacterial activity of polyoxometalates against *Moraxella catarrhalis*. *Front. Chem.* **6**, 336 (2018).

79. Suliman Mohamed, M., Timan Idriss, M., Khedr, A. I., Abd AlGadir, H., Takeshita, S., Shah, M. M., Ichinose, Y. & Maki, T. Activity of *Aristolochia bracteolata* against *Moraxella catarrhalis*. *Int. J. Bacteriol.* **2014** (2014).

Author contributions

AAAA: conceptualization, methodology, software, project administration. AAAA-M: data curation, formal analysis. AAAA-M: writing—original draft preparation, Abdullah Ahmed Ali Ahmed: final manuscript writing. AAAA-M, and JMAA: biological measurements. AAAA, SASQ, NSA, FAAS, and MS: visualization, investigation and validation. AAAA, AMA, and SASQ: visualization, supervision. AAAA and SASQ: writing—reviewing and editing.

Competing interests

The authors declare no competing interests.

Additional information

Correspondence and requests for materials should be addressed to A.A.A.A.

Reprints and permissions information is available at www.nature.com/reprints.

Publisher's note Springer Nature remains neutral with regard to jurisdictional claims in published maps and institutional affiliations.



Open Access This article is licensed under a Creative Commons Attribution 4.0 International License, which permits use, sharing, adaptation, distribution and reproduction in any medium or format, as long as you give appropriate credit to the original author(s) and the source, provide a link to the Creative Commons licence, and indicate if changes were made. The images or other third party material in this article are included in the article's Creative Commons licence, unless indicated otherwise in a credit line to the material. If material is not included in the article's Creative Commons licence and your intended use is not permitted by statutory regulation or exceeds the permitted use, you will need to obtain permission directly from the copyright holder. To view a copy of this licence, visit <http://creativecommons.org/licenses/by/4.0/>.

© The Author(s) 2023